

Angular clustering in the SUMSS radio survey

Chris Blake^{1,*}, Tom Mauch² and Elaine M. Sadler²

¹ *School of Physics, University of New South Wales, Sydney, NSW 2052, Australia*

² *School of Physics, University of Sydney, Sydney, NSW 2006, Australia*

10 November 2018

ABSTRACT

We measure the angular correlation function of radio galaxies selected by the 843 MHz Sydney University Molonglo Sky Survey (SUMSS). We find that the characteristic imprint of large-scale structure is clearly detectable, and that the survey is very uniform. Through comparison with similar analyses for other wide-area radio surveys – the 1400 MHz NRAO VLA Sky Survey (NVSS) and the 325 MHz Westerbork Northern Sky Survey (WENSS) – we are able to derive consistent angular clustering parameters, including a steep slope for the clustering function, $w(\theta) \propto \theta^{-1.1}$. We revise upwards previous estimates of the NVSS clustering amplitude, and find no evidence for dependence of clustering properties on radio frequency. It is important to incorporate the full covariance matrix when fitting parameters to the measured correlation function. Once the redshift distribution for mJy radio galaxies has been determined, these projected clustering measurements will permit a robust description of large-scale structure at $z \sim 0.8$, the median redshift of the sources.

Key words: large-scale structure of Universe – galaxies: active – surveys

1 INTRODUCTION

Recent deep, wide-area radio surveys have made it possible to measure the patterns of angular clustering in the radio sky. Radio selection provides a window on the galaxy distribution that differs significantly from optical wavebands. Radio sources probe the high-redshift universe: the broadness of the radio luminosity function ensures that the detected distribution of objects has a median redshift $\bar{z} \approx 0.8$, independently of flux-density threshold (Condon 1989). The projected clustering signal originates to a significant extent from redshift \bar{z} and serves as a robust tracer of structure at that epoch. However, the wide redshift range spanned carries a significant disadvantage: the angular clustering is vastly diluted by the superposition of unrelated redshift slices and hence the residual signal is faint, an order of magnitude smaller than the projected clustering of the faintest Sloan galaxies. Moreover, the apparent brightness of a radio galaxy provides no indication of its radial distance, whereas in optical wavebands galaxies have a characteristic luminosity that may be used to infer rough redshift information.

Radio selection is independent of Galactic and intergalactic extinction, so that reliably complete catalogues can be obtained over large areas. Even so, measuring the faint imprint of clustering has only been possible in the latest generation of surveys: Faint Images of the Radio Sky at Twenty

centimetres (FIRST, Becker, White & Helfand 1995), the Westerbork Northern Sky Survey (WENSS, Rengelink et al. 1997) and the NRAO VLA Sky Survey (NVSS, Condon et al. 1998). Each of these databases lists $> 10^5$ objects over $\sim 10,000 \text{ deg}^2$ to limiting flux densities $S_{1400 \text{ MHz}} \sim 3 \text{ mJy}$. The surveys differ in observing frequencies and angular resolution, thus inter-comparisons can reveal subtle instrumental and selection effects in individual catalogues (Blake & Wall 2002b).

A recent addition to this complementary suite of surveys is the 843 MHz Sydney University Molonglo Sky Survey (SUMSS). This is the first deep wide-area radio survey mapping the southern skies; and it does so at a frequency intermediate between that of WENSS (325 MHz) and NVSS (1400 MHz). Large-scale structure in the WENSS, FIRST and NVSS surveys has been quantified by various authors: Cress et al. (1996), Magliocchetti et al. (1998), Rengelink & Röttgering (1999), Blake & Wall (2002a, 2002b) and Overzier et al. (2003). In this study we apply a first clustering analysis to the SUMSS radio survey and compare the results with those derived from NVSS and WENSS, thus testing whether clustering is a function of radio frequency.

It is worth emphasizing that clustering studies serve as a rigorous test of the calibration and large-scale uniformity of a catalogue. In particular, the angular correlation function $w(\theta)$ analyzes the structure present as a function of angular scale θ . Instrumental effects in a radio survey typically manifest themselves on particular characteristic scales, and are

* E-mail: chrisb@phys.unsw.edu.au

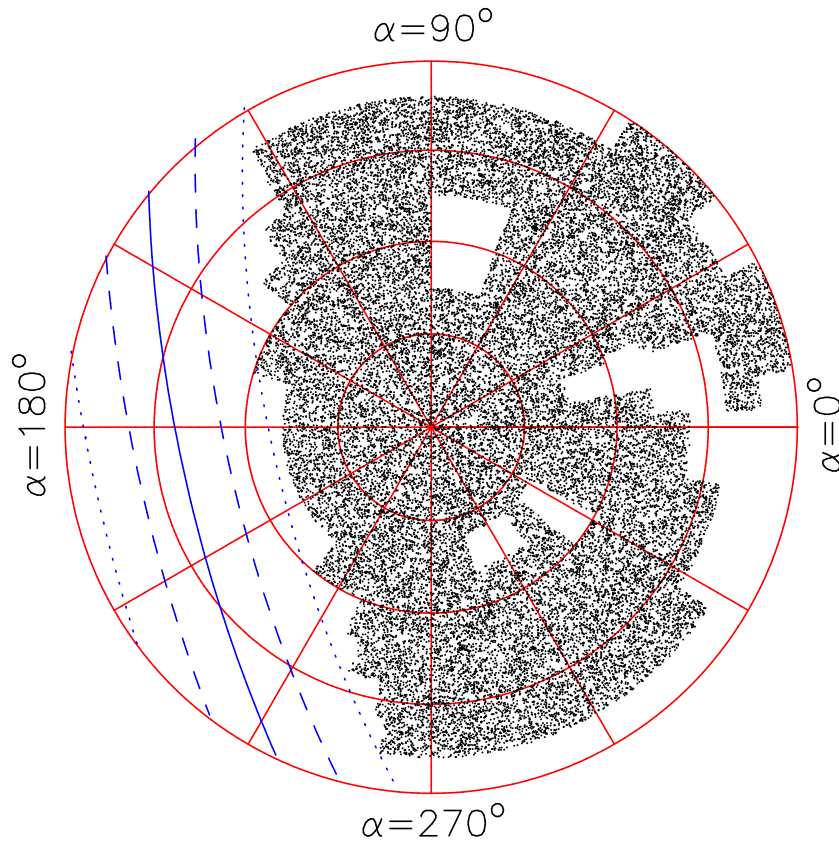


Figure 1. A plot of SUMSS catalogue entries with integrated fluxes exceeding 20 mJy in the region analyzed for large-scale structure. The outer circumference represents declination $\delta = -50^\circ$ and the centre of the diagram is $\delta = -90^\circ$, circles being plotted every 10 degrees. Galactic latitudes $b = 0^\circ, \pm 5^\circ$ and $\pm 10^\circ$ are marked on the plot as respectively solid, dashed and dotted lines.

usually rendered transparent by such an analysis. For example, unexpected features in the clustering pattern within the NVSS led to corrections to the data analysis pipeline for that survey (Blake & Wall 2002b).

To de-project the angular clustering amplitude and recover the true spatial clustering properties of the sample, we need to know the redshift distribution of the sources, $N(z)$. The radio source population at mJy flux-density levels is a mixture of nearby star-forming galaxies and more distant Active Galactic Nuclei (AGN) (Condon 1989). For example, approximately 5 per cent of NVSS sources are detected in the 2dF Galaxy Redshift Survey (Sadler et al. 2002), and 40 per cent of these are star-forming. The 95 per cent of NVSS galaxies not associated with 2dFGRS galaxies are overwhelmingly radio AGN with redshifts $z > 0.2$, which implies that ~ 98 per cent of NVSS radio sources are distant AGN. As their optical counterparts are often extremely faint, $N(z)$ has not yet been measured for radio AGN at mJy flux-density levels.

However, constraints on $N(z)$ exist from luminosity-function models, and utilizing these (with large extrapolations) we can estimate the present-day clustering length r_0 of radio galaxies (e.g. Magliocchetti et al. 1998, Blake & Wall 2002a, Overzier et al. 2003). The values inferred, in the range $r_0 = 7 \rightarrow 10 h^{-1}$ Mpc, correspond to a clustering strength intermediate between normal galaxies and rich clusters, consistent with the nature of radio AGN as optically-luminous elliptical galaxies inhabiting moderately

rich environments. An additional aim of this study is to establish the “best value” of the projected clustering amplitude of radio galaxies, to be employed in a more rigorous derivation of the clustering length when $N(z)$ is known.

2 THE SUMSS CATALOGUE

2.1 Summary

The Sydney University Molonglo Sky Survey (SUMSS) is imaging the southern ($\delta < -30^\circ$) radio sky at an observing frequency of 843 MHz. The survey uses the Molonglo Observatory Synthesis Telescope (MOST), a 1.6-km long cylindrical paraboloid reflector located near Canberra in Australia. The angular resolution of the SUMSS mosaics is $45'' \times (45'' \text{cosec}|\delta|)$. The survey design and science goals are described by Bock et al. (1999); observations began in 1997 and completion is scheduled for the end of 2003. The first instalment of the SUMSS source catalogue was presented by Mauch et al. (2003), who showed that it is complete to flux density $S_{843 \text{ MHz}} = 8$ mJy for declinations $\delta < -50^\circ$ and 18 mJy for $\delta > -50^\circ$. SUMSS has comparable sensitivity and resolution to the 1400 MHz NRAO VLA Sky Survey (NVSS) in the north ($\delta > -40^\circ$).

This clustering study uses Version 1.0 of the SUMSS source catalogue, dated 25 February 2003, available online at www.astrop.physics.usyd.edu.au/sumsscat. This ver-

sion of the catalogue covers approximately 3500 deg^2 of the southern sky and contains 107,765 entries. We restricted our analysis to the region $\delta < -50^\circ$, which has a significantly fainter completeness limit than $\delta > -50^\circ$, and we placed additional angular masks around the locations of the Magellanic Clouds: ($5^\circ < \alpha < 15^\circ$, $-75^\circ < \delta < -65^\circ$) and ($70^\circ < \alpha < 90^\circ$, $-75^\circ < \delta < -65^\circ$). Raw SUMSS images contain artefacts, grating rings and radial spokes (Bock et al. 1999), typically located near very bright sources. SUMSS identifies these image artefacts using a reliable decision tree algorithm; however, to be conservative, we placed circular masks of diameter 1° around catalogued sources brighter than 1 Jy. After these masking procedures, 68,373 catalogue entries remained with flux densities $S_{843 \text{ MHz}} > 8 \text{ mJy}$. This version of the SUMSS catalogue excludes fields located at Galactic latitudes $|b| < 10^\circ$, thus we can assume that the vast majority of the objects are extragalactic in origin. The sky distribution of the 20 mJy sample is plotted in Figure 1.

The overlap region of SUMSS and NVSS ($-40^\circ < \delta < -30^\circ$) permits some comparisons and cross-checks. The fraction of SUMSS sources missing from the NVSS catalogue is ≈ 0.5 per cent, the majority of which are artefacts left behind by the decision tree (these generally appear close to very bright sources which are masked in this study as described above). Furthermore, cross-matched radio sources have a median spectral index $S_\nu \propto \nu^{-0.8}$ (Mauch et al. 2003 Figure 8), consistent with previous determinations at $\nu \sim 1 \text{ GHz}$.

2.2 Uniformity of the SUMSS catalogue

Spurious fluctuations in source surface density within a survey cause systematic offsets in clustering measurements, unless these fluctuations can be accurately modelled. Large-scale density gradients with a magnitude of $\gtrsim 5$ per cent will drown out the cosmological signal in the angular correlation function on scales $\theta \gtrsim 1^\circ$, as we discuss in Section 4.2. In a wide-area survey undertaken with an interferometer such as the Very Large Array, large-scale gradients typically appear as a function of declination (Blake & Wall 2002a), because the projection of the interferometric baselines on the sky inevitably changes as a function of declination, whereas in principle all right ascensions can be observed at transit. Furthermore, the “snapshot” radio images used to construct a survey such as the NVSS have relatively sparse uv -plane coverage and require considerable processing and cleaning to remove artefacts. In contrast, the uv -coverage of SUMSS images is inherently continuous owing to the nature of the MOST: deconvolution is practically unnecessary and image cleaning is trouble-free (Bock et al. 1999).

Figure 2 plots the source surface density of the SUMSS catalogue as a function of declination for flux-density thresholds 8 mJy, 15 mJy and 30 mJy. There are no apparent spurious gradients as a function of declination, although the scatter of the data points exceeds that predicted by Poisson statistics (the error bars). This excess variance is produced by clustering, by multiple-component sources and (potentially) by spurious fluctuations in surface density. We placed a quantitative upper limit on the rms spurious density fluctuations by assuming that these were entirely responsible for the excess variance. We modelled the surface density at

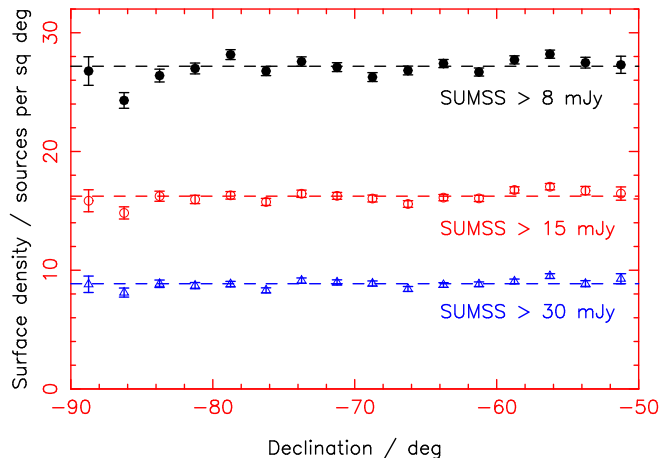


Figure 2. SUMSS source surface density as a function of declination. Sources are binned in declination bands for flux-density thresholds 8 mJy (solid circles), 15 mJy (open circles) and 30 mJy (triangles). The dashed lines indicate the average surface density at each threshold. The error in the number of sources N in a band is plotted as the “Poisson error” \sqrt{N} . Masked areas are excluded from this analysis.

declination δ as a sum of two components, $\sigma(\delta) = \sigma_0 + \sigma_1(\delta)$, where σ_0 is a constant-density “unperturbed” level and $\sigma_1(\delta)$ is a fluctuating offset (such that $\overline{\sigma_1} = 0$). The variance of the measured density over the declination bins is the sum of a “Poisson” contribution (due to σ_0) and a “systematic” contribution (due to σ_1). We derived the variance of σ_1 by subtracting the contribution of Poisson statistics from the total variance; the fractional rms fluctuation is then $f_{\text{fluc}} = \sqrt{\text{Var}(\sigma_1)}/\sigma_0$. The resulting upper limits on spurious density fluctuations in the SUMSS catalogue are respectively 2.2%, 2.0% and 2.5% at thresholds 8 mJy, 15 mJy and 30 mJy.

A systematic variation in surface density σ creates an approximately constant offset in $w(\theta)$ of magnitude ϵ^2 , where $\epsilon = (\sigma - \bar{\sigma})/\bar{\sigma}$ is the surface overdensity (Blake 2002). Thus we can write:

$$\Delta w(\theta) = \overline{\epsilon^2} = \frac{\text{Var}(\sigma_1)}{\sigma_0^2} = (f_{\text{fluc}})^2 \quad (1)$$

Our measurements detailed in the previous paragraph therefore placed an upper limit $\Delta w(\theta) \approx (0.02)^2 = 4 \times 10^{-4}$ on the effect of source density gradients in SUMSS. Thus our determination of $w(\theta)$ in Section 3 is not significantly affected by any such gradients.

3 ANGULAR CORRELATION FUNCTION FOR THE SUMSS CATALOGUE

We quantified the projected clustering in the SUMSS catalogue using the angular correlation function, $w(\theta)$. This two-point statistic is determined by counting the number of pairs of catalogue entries, $DD(\theta)$, as a function of angular separation θ , and comparing the result to the number of pairs expected by random chance. The value of $w(\theta)$ is the fractional enhancement of pair counts above random. We computed $w(\theta)$ using the Landy-Szalay estimator (Landy

& Szalay 1993). Using the Hamilton estimator (Hamilton 1993) led to identical results. The error in each separation bin is plotted in the Figures as a ‘‘Poisson’’ error:

$$\Delta w(\theta) = \frac{1 + w(\theta)}{\sqrt{DD(\theta)}} \quad (2)$$

This is known to be a very good approximation for the variance of this estimator of the correlation function.

When fitting models to the measured $w(\theta)$, we used the full covariance matrix of the separation bins, C_w . The covariance matrix for a given correlation function model was derived using the analytic approximation of Bernstein (1994, equation 39), who presents a specific treatment of the Landy-Szalay estimator; see also Eisenstein & Zaldarriaga (2001). Bernstein’s approximations – $N \gg 1$, $w(\theta) \ll 1$, $w_\Omega \ll w(\theta)$ – are valid for the present surveys. We made an additional approximation by neglecting higher-order correlations ($q = 0$). Once the correlation matrix has been computed, the chi-squared statistic is given by

$$\chi^2 = \Delta \mathbf{w}^T C_w^{-1} \Delta \mathbf{w} \quad (3)$$

where $\Delta \mathbf{w}$ is a vector containing the differences between the measured values of $w(\theta)$ and the model.

Apparent clustering in radio source catalogues is due to two effects: the cosmological clustering of separate galaxies, and the resolution of individual radio galaxies into multiple components which appear as separate catalogue entries. A $w(\theta)$ analysis neatly separates these two contributions. Excess pairs with separations $\theta \lesssim 0.1^\circ$ are almost exclusively produced by multiple components; cosmological effects predominate on scales $\theta \gtrsim 0.1^\circ$. A good fitting formula for the $w(\theta)$ data is a sum of two power-laws with sharply differing slopes, resulting in a clear break at $\theta \approx 0.1^\circ$ (see Blake & Wall 2002a and Overzier et al. 2003 for further justification of this model).

These effects are, as anticipated, present in the SUMSS catalogue. Figure 3 plots measurements of the SUMSS $w(\theta)$ at flux-density thresholds 8 mJy (which is the completeness limit) and 15 mJy. At 8 mJy, a sum of two power-laws is not in fact a good fit to the data points (for $\theta > 0.02^\circ$), with a minimum reduced chi-squared statistic $\chi_{\text{red}}^2 = 2.16$ (derived using the full covariance matrix; the probability that χ^2 should exceed this value by chance is $Q = 1.0 \times 10^{-3}$). However, at 10 mJy the fit has improved to $\chi_{\text{red}}^2 = 1.66$ ($Q = 0.024$) and the corresponding value for 20 mJy is $\chi_{\text{red}}^2 = 1.37$ ($Q = 0.11$). The poor fit at 8 mJy is probably due to unidentified systematic effects near the completeness limit of the survey, and we used the more conservative threshold of 10 mJy for subsequent analysis (see Section 4.3).

We investigated the dependence on flux density of the two power-laws used to model $w(\theta)$. As suggested by Figure 3 and quantified in Section 4.4, we found no change with flux density in the amplitude of the shallower power-law, which dominates on scales $\theta \gtrsim 0.1^\circ$ and reflects cosmological clustering. This finding is in agreement with other wide-area radio surveys in the flux density range $3 \text{ mJy} < S_{1400 \text{ MHz}} < 50 \text{ mJy}$. Note that this result is in sharp contrast to clustering measured in optical wavebands, where the clustering amplitude declines rapidly as galaxies become fainter. The explanation for this difference is simple: unlike in optical wavebands, fainter radio galaxies are not (on average) more dis-

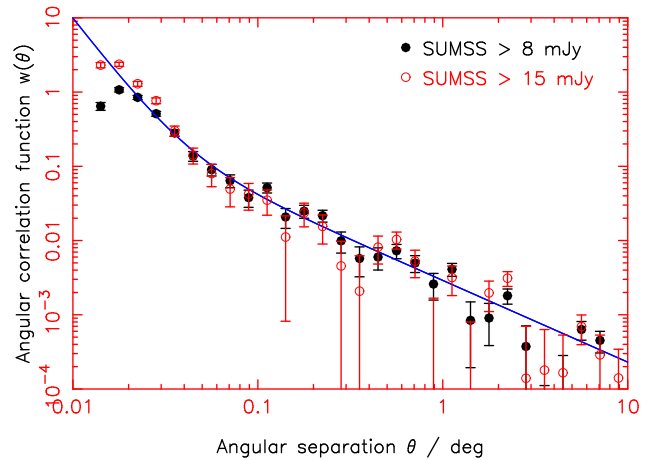


Figure 3. Measurement of the SUMSS angular correlation function at flux-density thresholds $S_{843 \text{ MHz}} = 8 \text{ mJy}$ (solid circles) and 15 mJy (open circles). The best-fitting sum of two power-laws for the 8 mJy data is overplotted. This is not a good fit, and we preferred to use a more conservative threshold of 10 mJy for the subsequent analysis.

tant. As shown in Figure 3, the multiple-components piece of $w(\theta)$ (at small separations) has an amplitude that decreases with flux density. Blake & Wall (2002a) demonstrated that the expected dependence of this amplitude is $1/\sigma$, where σ is the source surface density.

At very small separations $\theta < 0.02^\circ$ there is a fall-off in the value of $w(\theta)$ with decreasing θ . This is not real, but is a signal-to-noise effect caused by the failure of the survey to resolve weak double sources with separations slightly greater than the beam-width. At very large separations $\theta \approx 10^\circ$, the value of $w(\theta)$ is consistent with zero. This is strong evidence for a high degree of uniformity in the survey: as detailed in Section 2.2, calibration gradients produce spurious offsets in the value of $w(\theta)$.

4 COMPARISON WITH OTHER WIDE-AREA RADIO SURVEYS

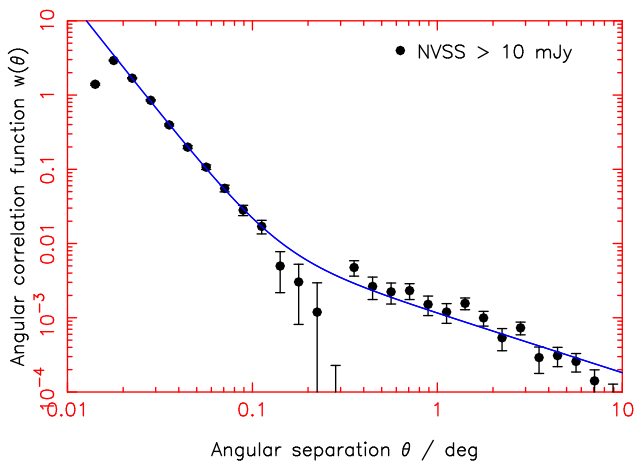
In this Section we compare the SUMSS clustering results with equivalent analyses of the 1400 MHz NRAO VLA Sky Survey (NVSS, Condon et al. 1998) and the 325 MHz Westerbork Northern Sky Survey (WENSS, Rengelink et al. 1997). These different samples are summarized in Table 1. The three surveys have comparable angular resolutions but different observing frequencies, potentially probing different selections of the radio source population. It is of interest to discover whether clustering is a function of radio frequency. Cosmological clustering of radio galaxies is independent of flux density in the range $3 \text{ mJy} < S_{1400 \text{ MHz}} < 50 \text{ mJy}$ (Section 4.4), thus the choice of comparison flux-density threshold for NVSS and WENSS is not important.

4.1 NVSS

The angular correlation function for NVSS has been measured by Blake & Wall (2002a) and Overzier et al. (2003). The result of Blake & Wall for flux-density threshold

Table 1. Summary of radio source samples used in this investigation.

Survey	Frequency (MHz)	Angular resolution (arcsec)	Declination range	Angular area (deg ²)	Flux density (mJy)	Number of sources	Surface density (deg ⁻²)
SUMSS	843	$45 \times (45 \operatorname{cosec} \delta)$	$-90^\circ < \delta < -50^\circ$	2,516	> 8	68,373	27.2
					> 10	57,071	22.7
					> 15	40,843	16.2
					> 30	22,301	8.9
NVSS	1400	45	$-40^\circ < \delta < 90^\circ$	31,104	> 10	524,808	16.9
WENSS	325	$54 \times (54 \operatorname{cosec} \delta)$	$30^\circ < \delta < 75^\circ$	8,409	> 35 (int)	107,937	12.8
			$30^\circ < \delta < 60^\circ$	6,579	> 35 (peak)	87,501	13.3


Figure 4. Measurement of the NVSS angular correlation function at flux-density threshold $S_{1400 \text{ MHz}} = 10 \text{ mJy}$, from Blake & Wall (2002a). The best-fitting sum of two power-laws is overplotted. This is not a good fit owing to a deficit of pairs with separations $\theta \approx 0.2^\circ$.

$S_{1400 \text{ MHz}} = 10 \text{ mJy}$ is plotted in Figure 4; this is the deepest flux density for which systematic surface density gradients are negligible. A sum of two power-laws is an excellent fit to the data points, except for separations $0.1^\circ < \theta < 0.3^\circ$, for which there is a significant deficit of pairs. This results in the overall best fit being poor ($\chi_{\text{red}}^2 = 2.21$, $Q = 7.0 \times 10^{-4}$).

We made the following improvement to previous analyses of the NVSS $w(\theta)$: we suggest that the data points at $\theta \approx 0.2^\circ$ are suspect. The NVSS synthesized beam features very strong, broad diffraction spikes (sidelobes) offset by $0.2^\circ \rightarrow 0.3^\circ$ from the main lobe, with amplitudes which are almost 30 per cent of the peak (Condon et al. 1998 Section 4.1 and Figure 17). These diffraction features correspond to the shortest baselines used in the VLA observations, which are about 37 metres (≈ 170 wavelengths).

It is very plausible that the required deep cleaning of the NVSS images causes the small deficit of galaxy pairs with separations $\theta \approx 0.2^\circ$. The consequent CLEAN bias will not remove 10 mJy sources near stronger sources, but it might reduce the flux density of the fainter source in each 0.2° pair by some fraction of the rms noise, which is $\sigma_{\text{noise}} = 0.5 \text{ mJy}$, independent of the true source flux density (J. Condon, priv. comm.). The observed shortfall of 0.2° pairs is ≈ 1 per cent (Figure 4). In comparison, the number of data pairs in the separation range $0.1^\circ < \theta < 0.3^\circ$ is increased by 1.6 per cent when the flux-density threshold is reduced by $\sigma_{\text{noise}}/5$ from

10.0 mJy to 9.9 mJy; we conclude that the shortfall of 0.2° pairs is probably an instrumental effect.

The effect of the deficit of pairs with separations $\theta \approx 0.2^\circ$ is to reduce spuriously the amplitude of the fitted clustering power-law, which must attempt to accommodate these low points. Fitting the clustering power-law to the separation range $\theta = 0.3^\circ \rightarrow 10^\circ$ instead, a much better fit to the data was obtained ($\chi_{\text{red}}^2 = 1.07$, $Q = 0.38$) with a clustering amplitude ~ 50 per cent higher than previously recorded. We postpone further discussion of the best-fitting clustering parameters to Section 4.3.

Overzier et al. (2003) describe an “unexplained bump” at separations $0.1^\circ < \theta < 0.3^\circ$ in the NVSS $w(\theta)$ measured above a threshold of 200 mJy. This is very probably an additional consequence of the diffraction sidelobes.

4.2 WENSS

The first measurements of the WENSS angular correlation function were presented by Rengelink & Röttgering (1999); we performed our own investigation. We analyzed the “main” WENSS catalogue, which covers the region $0^\circ < \alpha < 360^\circ$, $30^\circ < \delta < 75^\circ$, and is available online at www.strw.leidenuniv.nl/~dpf/wenss. The catalogue lists merged multiple-component (“M”) sources as well as their separate components (“C”) sources; we omitted the “M” sources. In addition we masked areas within 5° of the Galactic plane, and inside a large box ($15^\circ \times 15^\circ$) surrounding the bright radio source Cygnus A.

The completeness limit of WENSS has been determined as $S_{325 \text{ MHz}} = 35 \text{ mJy}$ (Rengelink & Röttgering 1999). Figure 5 plots the WENSS catalogue surface density at this limit as a function of declination in two different ways: firstly for a 35 mJy threshold in (deconvolved) integrated flux density, and secondly for a 35 mJy/beam threshold in (convolved) peak flux density. For a point source the integrated and peak flux densities are equal; the large WENSS beam ensures that these quantities do not usually differ significantly for catalogue entries.

For the threshold in integrated flux density in Figure 5, there is a systematic gradient amounting to a ~ 10 per cent fluctuation between $\delta = 30^\circ$ and $\delta = 75^\circ$. A possible explanation for this feature is that at higher declinations, the projection of the interferometric baselines on the sky is shorter, implying reduced surface brightness sensitivity and marginally reduced completeness as regards integrated flux. This surface density gradient creates a significant spurious offset in $w(\theta)$, drowning out the cosmological signal at sep-

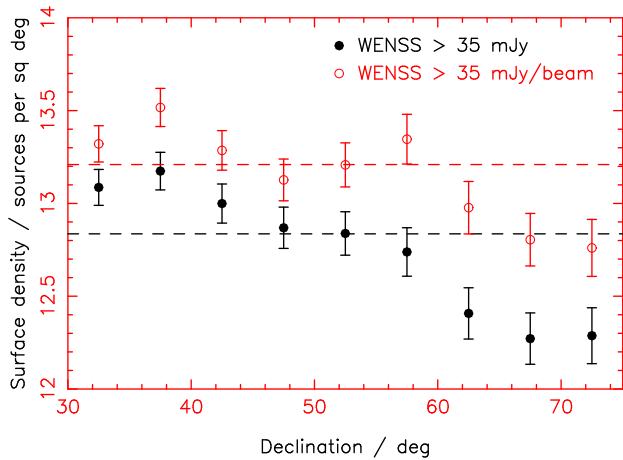


Figure 5. WENSS source surface density as a function of declination at integrated flux-density threshold 35 mJy (solid circles) and peak flux-density threshold 35 mJy/beam (open circles). The dashed lines indicate the average surface densities at these thresholds. The error in the number of sources N in a band is \sqrt{N} .

arations $\theta \gtrsim 1^\circ$ (see Figure 6). These systematic effects are much less serious for the sample selected by peak flux density. Thus, motivated by Figure 5, we created a more uniform WENSS source catalogue by imposing a peak flux-density threshold of 35 mJy/beam, and restricting our analysis to the declination band $30^\circ < \delta < 60^\circ$ (≈ 80 per cent of the available area).

Our measurements of the WENSS $w(\theta)$ for these two catalogue selections are displayed in Figure 6. For the peak flux-density threshold, a double power-law again provides a reasonable fit ($\chi^2_{\text{red}} = 1.50$, $Q = 6.4 \times 10^{-2}$). However, the influence of surface gradients is still not negligible and the angular correlation function at large separations ($\theta \sim 10^\circ$) is not consistent with zero. Therefore the best-fitting clustering power-law spuriously acquires a significantly shallower slope than that determined for SUMSS and NVSS. We therefore added an additional parameter – a constant offset – to the WENSS angular correlation function fitting formula. Although this extra parameter does not significantly improve the χ^2 statistic of the best-fitting model, it is well-motivated by the existence of the surface density gradients.

4.3 Comparison of clustering amplitudes

We compared the angular correlation functions for SUMSS (> 10 mJy), NVSS (> 10 mJy) and WENSS (> 35 mJy/beam) (Figure 7). We used the 10 mJy threshold for SUMSS (rather than the completeness limit of 8 mJy) because 10 mJy is the deepest flux-density level for which a power-law model proved a good fit to the data.

We fitted a power-law $w(\theta) = A\theta^{-\alpha}$ to the cosmological clustering part of each correlation function, using the full covariance matrix. In the case of WENSS, we introduced a third variable parameter, a constant offset, to accommodate the surface gradients. The angular ranges to which the functions were fitted were $\theta > 0.2^\circ$ (SUMSS, WENSS) and $\theta > 0.3^\circ$ (NVSS). For SUMSS and WENSS, $\theta > 0.2^\circ$ safely exceeds separations for which multiple component sources are important ($\theta \lesssim 0.1^\circ$). For NVSS, $\theta > 0.3^\circ$ also avoids

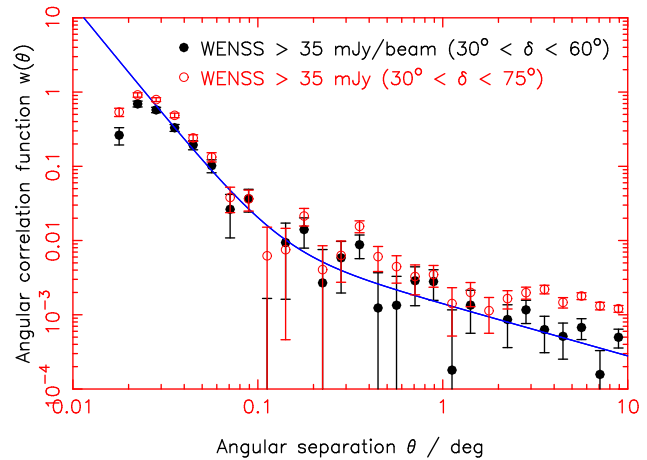


Figure 6. Measurement of the WENSS angular correlation function. The open circles plot the result for integrated flux-density threshold $S_{325\text{MHz}} = 35$ mJy over declination range $30^\circ < \delta < 75^\circ$. A spurious offset is evident for separations $\theta \gtrsim 1^\circ$ due to a source surface density gradient. This motivated us to select a more uniform catalogue by imposing a 35 mJy/beam threshold in peak flux density over the area bounded by $30^\circ < \delta < 60^\circ$. The $w(\theta)$ result for this second selection is plotted as the solid circles, together with the best-fitting double power-law model.

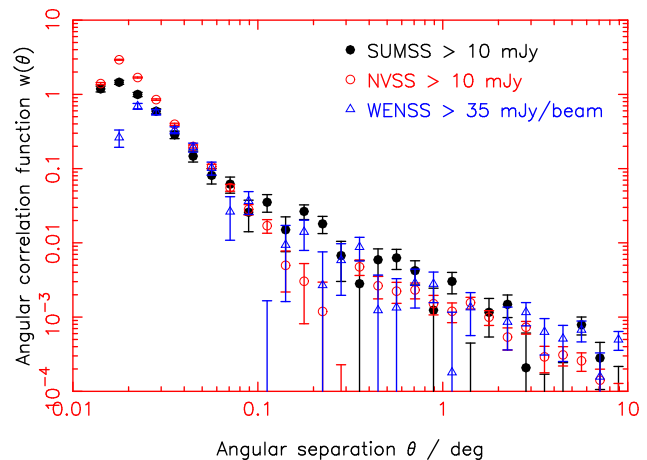


Figure 7. Overplot of the angular correlation functions for SUMSS (> 10 mJy, solid circles), NVSS (> 10 mJy, open circles) and WENSS (> 35 mJy/beam, triangles).

the influence of diffraction spikes at $\theta \approx 0.2^\circ$. Figure 8 plots contours of constant χ^2 in the space of the clustering parameters (A , α). The results for the three independent surveys are consistent; there is no evidence that clustering is a function of observing frequency.

The best-fitting clustering parameters for the three surveys are tabulated in Table 2. They differ somewhat from those previously reported for the NVSS, which were $A = (1.0 \pm 0.2) \times 10^{-3}$, $\alpha = 0.8 \pm 0.1$ (Blake & Wall 2002a, Overzier et al. 2003; note that θ is measured in degrees for all quoted values of the amplitude A). These differences are due to ignoring the low $w(\theta)$ data at $\theta \approx 0.2^\circ$ in the NVSS measurement. The best-fitting slope is now somewhat higher, $\alpha \approx 1.1$, agreeing with the value originally reported for the FIRST survey by Cress et al. (1996). In fact, it is not sur-

Table 2. Results of power-law fits to the cosmological clustering part of the angular correlation function, $w(\theta) = A\theta^{-\alpha}$, for SUMSS, NVSS and WENSS. In the case of WENSS a constant offset is also fitted to the function. The best fit is obtained by minimizing the χ^2 statistic, incorporating the full covariance matrix. The errors in the parameters are derived by varying each in turn from the best-fitting combination (keeping the others fixed) and determining the variation for which $\Delta\chi^2 = 1$, the appropriate 1-sigma increment when varying one fitted parameter.

Survey	Flux density (mJy)	Amplitude A ($\times 10^{-3}$)	Slope α	Constant offset ($\times 10^{-3}$)	χ^2_{red}	Q
SUMSS	> 10	2.04 ± 0.38	1.24 ± 0.16	–	1.79	0.03
NVSS	> 10	1.49 ± 0.15	1.05 ± 0.10	–	0.89	0.57
WENSS	> 35 (peak)	1.01 ± 0.35	1.22 ± 0.33	0.35 ± 0.19	1.37	0.15

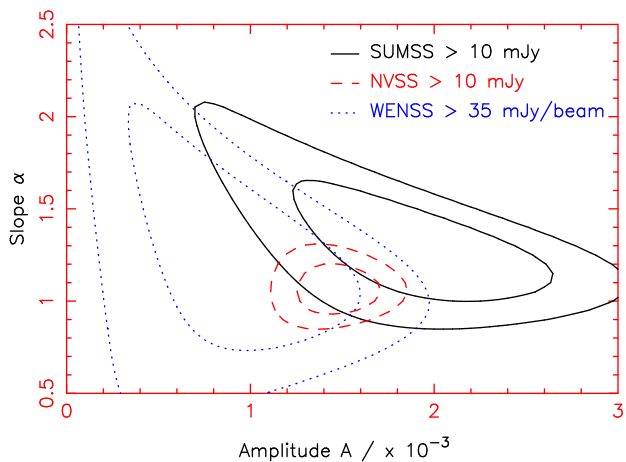


Figure 8. Measurement of the clustering parameters $w(\theta) = A\theta^{-\alpha}$ for SUMSS (solid line), NVSS (dashed line) and WENSS (dotted line). Contours of constant χ^2 are shown in the space of the parameters (A, α), corresponding to 1σ and 2σ confidence regions. As the plot is in the space of two varying parameters, the 1σ and 2σ contours are defined by χ^2 increasing by respectively 2.30 and 6.17 from its minimum. When generating this plot, the covariance matrix was held fixed at that corresponding to the best-fitting correlation function model.

prising that the clustering slope should exceed the canonical value $\alpha = 0.8$ of normal galaxies; it is known that α depends on galaxy type and takes on its steepest value for elliptical galaxies such as radio AGN (Norberg et al. 2002). The new value of the clustering amplitude, $A \approx 1.6 \times 10^{-3}$, also exceeds the previous determination.

Inclusion of the full covariance matrix in the fitting procedure increases the errors on the clustering parameters by ~ 50 per cent, compared to the approximation of neglecting correlations between separation bins. This result holds despite the fact that the variances of each bin are dominated by Poisson noise rather than by cosmic variance.

The multiple-components piece of $w(\theta)$, at $\theta \lesssim 0.1^\circ$, varies between the three surveys (Figure 7). These differences are explained by the $1/\sigma$ dependence of the amplitude of the small-angle $w(\theta)$ on surface density σ , together with the small variations in angular resolution between the surveys.

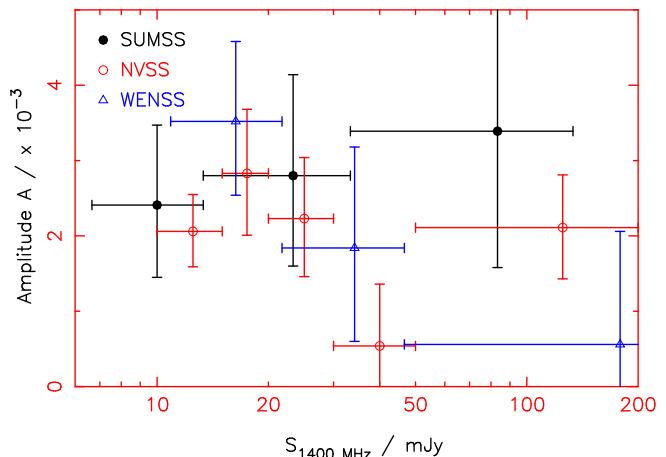


Figure 9. Angular correlation function amplitudes for SUMSS, NVSS and WENSS for various independent flux-density ranges. The slope of $w(\theta)$ was fixed at -1.1 in all cases.

4.4 Projected clustering amplitude as a function of flux density

We repeated the angular correlation function measurements for SUMSS, NVSS and WENSS for various independent flux-density ranges, and fitted a power-law $w(\theta) = A\theta^{-1.1}$ to the cosmological clustering parts of each function (keeping the slope fixed to permit comparison of amplitudes). We fitted an additional constant offset in the case of the WENSS analysis. The amplitudes are displayed in Figure 9; results at different observing frequencies have been transformed to 1400 MHz assuming a spectral index $S_\nu \propto \nu^{-0.8}$.

Figure 9 demonstrates that the amplitude of projected clustering does not depend on either observing frequency or flux density (for $S_{1400 \text{ MHz}} \lesssim 50$ mJy). At brighter flux densities the signal-to-noise of the measurement is too low to allow firm conclusions to be drawn. We note that Overzier et al. (2003) found evidence for an enhanced angular clustering amplitude in NVSS for a threshold $S_{1400 \text{ MHz}} = 200$ mJy, with a large error bar.

5 SUMMARY

The results of this investigation may be summarized as follows:

- The angular correlation function for the SUMSS radio

survey is measured for the first time and is found to have the same double power-law structure as previously identified in NVSS.

- Our analysis reveals no evidence for large-scale systematic gradients in SUMSS, such as might be imprinted by instrumental effects or data reduction.

- The NVSS $w(\theta)$ is re-examined, and data points on angular scales $0.1^\circ < \theta < 0.3^\circ$ are excluded from the fitting process due to the possible influence of imperfectly-cleaned bright sidelobes.

- The WENSS $w(\theta)$ is re-examined, and a systematic surface density gradient as a function of declination is identified for sources selected above a fixed threshold in integrated flux density. A more uniform source catalogue can be created by imposing a threshold in peak flux density.

- The parameters of the clustering power-law, $w(\theta) = A\theta^{-\alpha}$, derived for SUMSS, NVSS and WENSS, are found to be in agreement, having values $\alpha \approx 1.1$ and $A \approx 1.6 \times 10^{-3}$. Errors in the parameters for the individual surveys are mapped in Figure 8 and Table 2.

- Inclusion of the full covariance matrix of the separation bins significantly increases the errors on the fitted clustering parameters, compared to the assumption that the bins are statistically independent.

- We find no evidence for a dependence of projected clustering amplitude on either flux density or observing frequency.

The inter-comparison of these three wide-area radio surveys has resulted in the refinement of our knowledge of the projected clustering of radio galaxies. Once the redshift distribution of these sources has been determined at mJy flux-density levels, their angular clustering amplitude may be used to make a robust measurement of the spatial clustering of luminous elliptical galaxies at $z \approx 0.8$.

ACKNOWLEDGMENTS

We acknowledge useful discussions with Carole Jackson concerning radio source populations as a function of frequency, with Jim Condon concerning instrumental effects in the NVSS, and with Michael Brown concerning the covariance of correlation function estimates. We thank Jasper Wall, Roderik Overzier and Dick Hunstead for useful comments on earlier drafts of the manuscript. We acknowledge Roeland Rengelink for a very helpful referee's report.

REFERENCES

Becker R.H., White R.L., Helfand D.J., 1995, *ApJ*, 450, 559
 Bernstein G.M., 1994, *ApJ*, 424, 569
 Blake C.A., 2002, PhD thesis, University of Oxford
 Blake C.A., Wall J.V., 2002a, *MNRAS*, 329, L37
 Blake C.A., Wall J.V., 2002b, *MNRAS*, 337, 993
 Bock D.C.-J., Large M.I., Sadler E.M., 1999, *ApJ*, 117, 1578
 Condon J.J., 1989, *ApJ*, 338, 13
 Condon J.J., Cotton W.D., Greisen E.W., Yin Q.F., Perley R.A., Taylor G.B., Broderick J.J., 1998, *AJ*, 115, 1693
 Cress C.M., Helfand D.J., Becker R.H., Gregg M.D., White R.L., 1996, *ApJ*, 473, 7
 Eisenstein D.J., Zaldarriaga M., 2001, *ApJ*, 546, 2
 Hamilton A.J.S., 1993, *ApJ*, 417, 19

Landy S.D., Szalay A.S., 1993, *ApJ*, 412, 64
 Magliocchetti M., Maddox S., Lahav O., Wall J., 1998, *MNRAS*, 300, 257
 Mauch T., Murphy T., Buttery H.J., Curran J., Hunstead R.W., Pietrzynski B., Robertson J.G., Sadler E.M., 2003, *MNRAS*, 342, 1117
 Norberg et al., 2002, *MNRAS*, 332, 827
 Overzier R.A., Röttgering H.J.A., Rengelink R.B., Wilman R.J., 2003, *A&A*, 405, 53
 Rengelink R.B., Tang Y., de Bruyn A.G., Miley G.K., Bremer M.N., Röttgering H.J.A., Bremer M.A.R., 1997, *A&AS*, 124, 259
 Rengelink R.B., Röttgering H.J.A., 1999, in “The Most Distant Radio Galaxies”, ed. Röttgering H.J.A., Best P.N., Lehnert M.D., p.399
 Sadler E.M. et al., 2002, *MNRAS*, 329, 227